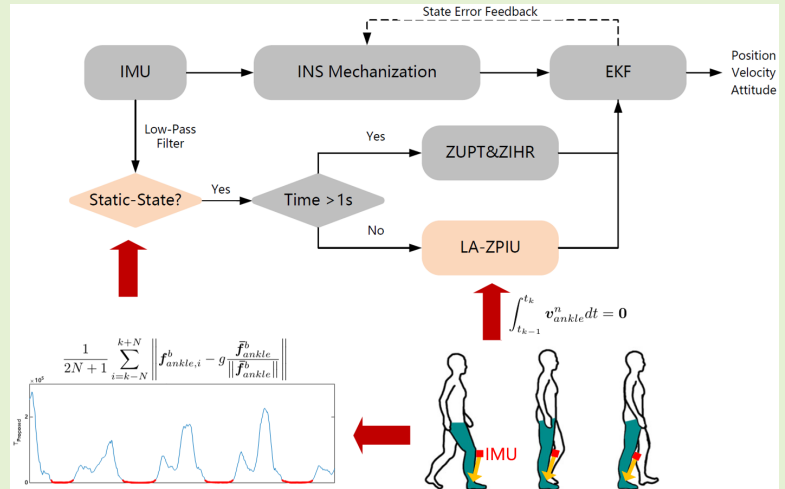


Shin-INS: A Shin-Mounted IMU-based Inertial Navigation System for Pedestrian

Jian Kuang, Dazhou Xia, Tao Liu, Qijin Chen, Xiaoji Niu

Abstract—Pedestrian dead reckoning, relying on an inertial measurement unit (IMU), plays a crucial role in the pedestrian positioning system. However, existing step model-based methods suffer from low positioning accuracy, and foot-mounted inertial navigation systems (Foot-INS) require specialized shoe, limiting their application to ordinary users. To address these issues, this paper introduces a shin-mounted inertial navigation system (Shin-INS) for pedestrians, leveraging an IMU. Firstly, a novel static state detector is proposed, enabling precise detection of the foot-ground contact state by projecting IMU observations to the ankle using lever-arm compensation. Additionally, the zero position increment update is employed to effectively mitigate velocity errors within the INS, thereby achieving accurate estimation of the user's position. Through tests conducted on both normal and abnormal walking scenarios, the results demonstrate that Shin-INS significantly enhances system installation convenience while achieving comparable positioning performance compared to Foot-INS.

Index Terms—Pedestrian dead reckoning (PDR), foot-mounted inertial navigation system (Foot-INS), shin-mounted inertial navigation system (Shin-INS), pedestrian navigation.



I. INTRODUCTION

PEDESTRIAN navigation systems (PNS) play a crucial role in ensuring the safety of workers in indoor environments, particularly during high-stakes situations like fire and emergency rescues [1]. Among the autonomous PNS methods, inertial measurement unit (IMU)-based pedestrian dead reckoning (PDR) stands out as it operates independently of prior information such as signal base stations or signal fingerprint databases, making it unaffected by external conditions [2]–[4]. The IMU-based PDR method relies on extracting regular characteristics of different body parts during normal walking and integrating IMU measurements to accurately estimate the user's pose. Two notable IMU-based PDR techniques are step model-based PDR (S-PDR) and foot-mounted inertial navigation systems (Foot-INS) [5]–[9].

S-PDR assumes that pedestrians move within a two-dimensional plane and utilizes IMU observations to estimate

the walking direction and empirical step length model to track the user's continuous position [3]. S-PDR is a versatile method that can be applied to IMUs mounted on various body parts such as handheld (i.e., smartphone) [3], wrist-mounted (i.e., smartwatch) [10], [11], helmet-mounted [12], chest-mounted [13], waist-mounted [14], pocket-mounted [15], [16], and foot-mounted [5], [6]. Although S-PDR described in the literature can achieve excellent positioning performance, the development of S-PDR faces two significant challenges. Firstly, a uniform step length estimation model that applies to all users is not readily available. Empirical step models, such as linear models [17], Weiberg models [18], and Kim models [19], etc., construct the functional correspondence between human body parameters (e.g., height and weight), motion parameters (e.g., step frequency, acceleration and swing angle of leg) and real distances, and can use low-precision sensors to stably estimate the user's walking distance. However, although the step length estimation model demonstrates high accuracy when trained on specific datasets, its performance significantly deteriorates when applied to unknown users, owing to factors such as height, weight, and walking habits variations [20]. Secondly, there is limited availability of accurate methods for estimating walking direction. In recent years, the research hotspot is the attitude and heading reference system (AHRS) that integrates

This work was supported by the Fundamental Research Funds for the Central Universities (2042023kf0124). (Corresponding author: Qijin Chen.)

J. Kuang, D. Xia, T. Liu, Q. Chen and X. Niu are with the GNSS Research Center, Wuhan University, Wuhan, Hubei, CO 430072 PR China. X. Niu is also with the Hubei LuoJia Laboratory. (E-mails: kuang@whu.edu.cn; dzhxia@whu.edu.cn; liu_tao@whu.edu.cn; chenqijin@whu.edu.cn; xjniu@whu.edu.cn).

gyroscopes, accelerometers, and magnetometers. The sensor heading estimation under complex environments and dynamic conditions can be significantly improved. However, due to the basic assumption adopted by S-PDR that the heading of the sensor is consistent with the walking direction of the user cannot be guaranteed, especially in the scene where the user walks along the sideways, transverse, and backward directions, accurately estimating the angle difference under complex user habit differences remains an unsolved problem [21], [22].

Compared with S-PDR, Foot-INS utilizes the user's foot dynamic information captured by the foot-mounted IMU to estimate the user's step length and walking direction, providing higher and more robust positioning performance [7], [23]. Foot-INS assumes periodic contact between the pedestrian's feet and the ground and utilizes zero-velocity update technology (ZUPT) to mitigate velocity errors in inertial navigation. Skog et al. proposed the generalized likelihood ratio test (GLRT), which detects the zero-velocity period by comprehensively utilizing the information that the angular rate is zero and the specific force is the projection of the gravitational acceleration [24]. GLRT is the most widely used threshold-based detection method for Foot-INS. Due to the obvious difference in detection accuracy of GLRT based on a fixed threshold in complex gait scenes, many researchers try to adjust the threshold adaptively according to the user's motion state. Wahlström et al. [25] proposed to use Bayesian theory and loss factors to determine the optimal threshold for different walking modes. Ren et al. [26] and Zhang et al. [27] established the relationship between linear velocity and optimal threshold. Tian et al. [28] determined the optimal threshold in different walking speeds according to the gait frequency. Ma et al. [29] established an angular velocity model to determine the optimal threshold in different walking states. The current zero-velocity detection methods have been able to meet the needs of normal gait scenarios of normal people, and the stability of Foot-INS has been significantly improved.

However, the heading estimation in Foot-INS is either unobservable or weakly observable when relying solely on ZUPT [30]. To address the issue of heading drift, various methods based on regular motion patterns have been proposed [23], [31], [32]. The zero integrated heading rate (ZIHR) is a basic heading constraint method that proves beneficial during extended periods of user inactivity, such as standing still [23]. Straight-line constraints utilize the observation that pedestrians tend to walk along straight lines between two points, effectively reducing the drift in walking direction [33]. Inspired by linear trajectory constraints, the heuristic drift elimination (HDE) method based on building orientation is proposed to control the heading drift error of Foot-INS [32], [34], [35]. HDE builds a heading fingerprint library by extracting building orientation, which can provide absolute heading observation information, but it is only applicable to the regular indoor corridor environment. Additionally, in outdoor environments, the absolute heading derived from magnetometer observations can maintain the Foot-INS heading within an acceptable error range, ensuring long-term stable position estimation. By combining these methods, the positioning performance and stability of Foot-INS have been significantly improved.

Indeed, Foot-INS has limitations in terms of its reliance on specialized shoes with built-in IMUs, which are typically suitable for specific individuals engaged in specialized tasks. Special shoes hinders the scalability of Foot-INS as they are specifically designed for binding with certain users, making them less adaptable to common application scenarios like tunnel inspections. Furthermore, the rigid contact between the foot and the ground in Foot-INS poses the risk of sensor saturation [36], [37], and the high dynamics of foot movements can introduce significant sensor dynamic errors. Additionally, the frequent impacts and weight exerted on the foot during operation can considerably shorten the sensor's lifespan. Considering these challenges, an alternative approach could involve mounting the IMU above the ankle to overcome the aforementioned issues while achieving similar positioning performance to Foot-INS. By relocating the IMU position, it may be possible to alleviate the scalability and saturation risks associated with foot-mounted sensors. This approach holds the potential to offer improved flexibility and usability without losing positioning performance in pedestrian navigation scenarios.

This paper introduces a shin-mounted inertial navigation system (Shin-INS) based on an IMU, offering comparable positioning performance to Foot-INS. Shin-INS employs a simple knee pad installation method, ensuring system convenience and making it feasible for widespread adoption of low-cost and high-precision PDR among the general population. Based on the objective fact that each position of shin undergoes a fixed-point rotation around the ankle when the foot is in contact with the ground, this paper utilizes lever arm compensation combined with IMU observation to calculate the ankle acceleration. On this basis, this paper proposes a novel zero-velocity detector based on a calf-mounted IMU. To address interference caused by the calf muscles, the paper presents a zero position incremental update method based on lever arm compensation (LA-ZPIU), which enables precise and stable position estimation while suppressing undesired influences. By leveraging these techniques, Shin-INS achieves accurate and reliable positioning while maintaining user convenience, making it a promising solution for widespread adoption in various applications.

The remainder of the paper is organized as follows: The movement analysis of human lower limbs is provided in Section II. Section III proposes a shin-mounted IMU based static period detection method. In Section IV, a Shin-mounted inertial navigation system is proposed. Section V presents the experimental results. Section VI discusses the performance of lever-arm estimation in the Shin-INS. Section VII summarizes the work of this paper and proposes a direction for future work.

II. MOVEMENT ANALYSIS OF HUMAN LOWER LIMBS

Figure 1 illustrates the continuous motion state of the foot during one step cycle. During normal walking, the foot can be categorized into dynamic and static periods. The static period refers to the phase when the foot is in contact with the ground, and its velocity is considered to be zero during this time. This assumption forms the basis for achieving

high-precision relative positioning in foot-mounted IMU-based pedestrian dead reckoning. Methods that utilize IMUs installed in non-foot positions often rely on empirical step models to compensate for the absence of zero-velocity correction [3], [10]–[16]. However, compared to foot-mounted inertial navigation systems (INS), the step model-based method suffers from significant performance degradation due to its poor applicability to different user motion behaviors.

Based on the analysis of a substantial amount of walking data from multiple users, we discovered that the relative position relationship between the shin-mounted IMU and the ankle remains constant throughout the step cycle. Figure 1 visually demonstrates this relative positional relationship between the shin and ankle during a step cycle. Although the Shin-IMU does not exhibit a strict static state during the foot cycle, it undergoes a fixed-point rotation around the ankle when the foot is in contact with the ground. Leveraging this motion criterion, we can project the IMU observations to the ankle and establish a zero-velocity constraint by utilizing the fact that the ankle's velocity should be zero. By incorporating this constraint, pedestrian dead reckoning (PDR) based on non-foot-position mounted IMUs can also achieve robust position estimation. This finding provides valuable insights into leveraging the continuous implicated motion between the shin and ankle, enabling the development of accurate and reliable PDR methods using IMUs placed in non-foot positions.

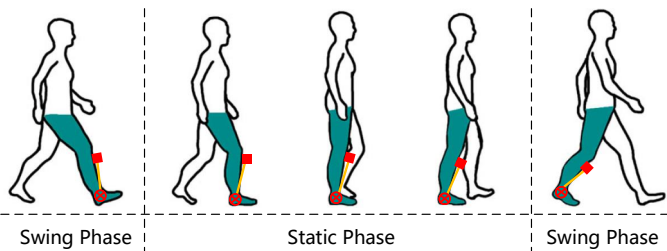


Fig. 1: The relative positional relationship between shin and ankle in a step cycle. The red square is the shin-mounted IMU, the red circle is ankle, and the orange dotted line is the relative position vector of the two.

III. STATIC PERIOD DETECTION BASED ON A SHIN-MOUNTED IMU

Assuming that an IMU is stably fixed at a certain position of shin, the relative positional relationship between the IMU and ankle is constant. The velocity relationship between IMU and ankle in the navigation frame (n -frame) can be expressed as [3]

$$\mathbf{v}_{ankle}^n = \mathbf{v}^n + \mathbf{C}_b^n (\boldsymbol{\omega}^b \times) \mathbf{l}^b \quad (1)$$

where \mathbf{v}_{ankle}^n and \mathbf{v}^n are the velocity at ankle and the shin-mounted IMU in the n -frame, respectively, \mathbf{C}_b^n is the transformation matrix from the body frame (b -frame) to the n -frame, $\boldsymbol{\omega}^b$ is angle rate output by the IMU, \mathbf{l}^b is the lever arm (the position vector from the center of IMU to ankle) in the b -frame.

Differentiating both sides of Eq. 1, we have

$$\dot{\mathbf{v}}_{ankle}^n = \dot{\mathbf{v}}^n + \dot{\mathbf{C}}_b^n (\boldsymbol{\omega}^b \times) \mathbf{l}^b + \mathbf{C}_b^n (\dot{\boldsymbol{\omega}}^b \times) \mathbf{l}^b \quad (2)$$

Subtracting the gravity vector from both sides of Eq. 2, and projecting into the b -frame has [37]

$$\mathbf{f}_{ankle}^b = \mathbf{f}^b + \underbrace{(\boldsymbol{\omega}^b \times) (\boldsymbol{\omega}^b \times) \mathbf{l}^b}_{\text{Centrifugal term}} + \underbrace{(\dot{\boldsymbol{\omega}}^b \times) \mathbf{l}^b}_{\text{Euler term}} \quad (3)$$

where \mathbf{f}_{ankle}^b and \mathbf{f}^b are the specific force of ankle and IMU in the b -frame, respectively, $\dot{\boldsymbol{\omega}}$ is the angular rate acceleration. We know that the specific force at ankle in the b -frame can be decomposed into the specific force of IMU, the centrifugal term, and the Euler term.

Based on the fact that the acceleration of ankle should be zero when the foot is in contact with the ground, the constructed static state detection criterion is given by

$$\frac{1}{2N+1} \sum_{i=k-N}^{k+N} \left\| \mathbf{f}_{ankle,i}^b - g \frac{\bar{\mathbf{f}}_{ankle}^b}{\|\bar{\mathbf{f}}_{ankle}^b\|} \right\| \leq \gamma_1 \quad (4)$$

where \mathbf{f}_{ankle}^b is the specific force at the ankle estimated by Eq. 3, $\bar{\mathbf{f}}_{ankle}^b = \frac{1}{2N+1} \sum_{i=k-N}^{k+N} \mathbf{f}_{ankle,i}^b$ is the mean specific force, γ_1 is the static state detection threshold set according to experience, $g = 9.8m/s^2$ is Earth's gravity, $2N+1$ is windows length for zero-velocity detection, $\|\cdot\|$ is the 2-norm of the vector. Since the conditions for accurate measurement of \mathbf{l}^b cannot be guaranteed for different users, γ_1 is usually set to roughly determine the motion state of the foot. The difference between the maximum and minimum within the zero-velocity period must satisfy a preset threshold is used to ensure zero-velocity period detection accuracy.

$$\text{Max}(\|\mathbf{f}_{ankle}^b\|_{k-N:k+N}) - \text{Min}(\|\mathbf{f}_{ankle}^b\|_{k-N:k+N}) \leq \gamma_2 \quad (5)$$

where γ_2 is the threshold set according to experience. To weaken sensor noise and high-frequency motion interference, IMU observations need to be low-pass filtered before being used to detect stationary states, with a cutoff frequency of 4 Hz.

Figure 2 presents the test statistics estimated by four traditional methods and the proposed method during normal walking. During the time period [6055, 6060], it is known that the foot equipped with a sensor touches the ground a total of four times. However, the test statistics obtained from $T_{|a|-Var}$, $T_{|a|}$, T_ω , and T_{SHOE} are all greater than 4 times, there is an obvious false detection results. The test statistics obtained by the proposed method are more clearly differentiated between static and dynamic, allowing the best identification of static periods. This improvement can be attributed to the fact that the position corresponding to the shin-mounted IMU does not possess a strict static state. By leveraging lever arm compensation, the proposed method achieves dynamic perception of the ankle, enabling more accurate detection of the static state at the signal level. Overall, the results showcased in Figure 2 highlight the superior performance of the proposed method in terms of distinguishing between the static and dynamic states during normal walking. The utilization of lever arm compensation facilitates more precise static state detection, addressing the challenges associated with the absence of a strict static state in the position where the shin-mounted IMU is installed.

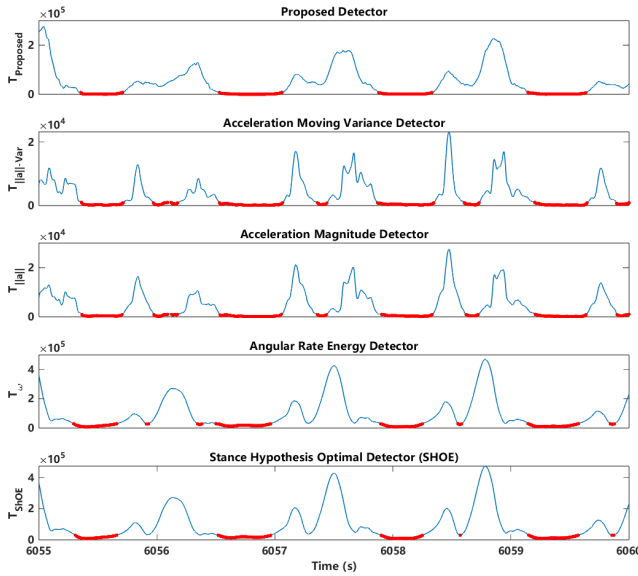


Fig. 2: Test statistics estimated by five methods in the normal walking state. The red dots are the detected stationary state moments. $T_{Proposed}$ is the proposed detector, $T_{||a||-Var}$ is acceleration moving variance detector, $T_{||a||}$ is acceleration magnitude detector, T_{ω} is angular rate energy detector, T_{SHOE} is stance hypothesis optimal detector (i.e., the classic method-GLRT). Specific calculation methods for different detectors can be found in [24].

IV. SHIN-MOUNTED INERTIAL NAVIGATION SYSTEM

The proposed zero-velocity detector plays a crucial role in providing periodic velocity observation information during normal walking, thus achieving a similar working condition to Foot-INS. The algorithm flow of Shin-INS is depicted in Figure 3. The INS Mechanization module estimates the user's position, velocity, and attitude by integrating the angular rate and specific force measurements from the IMU. Simultaneously, the navigation state is updated using three key components: lever arm-based zero position increment update (LA-ZPIU), zero velocity update (ZUPT), and zero integrated heading rate (ZIHR). These updates are performed based on the results obtained from the static state detection, ensuring robust estimation of the pedestrian's position.

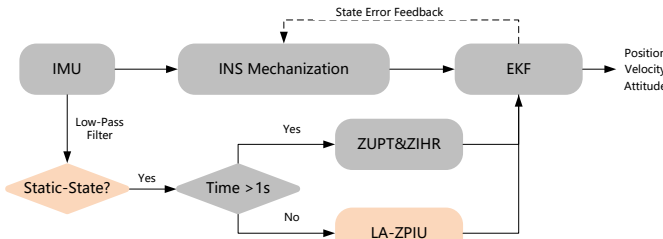


Fig. 3: Algorithm flow of Shin-INS.

A. Inertial Navigation Algorithm

INS mechanization is a typical inertial navigation algorithm, and the entire solution process has very rigorous theoretical

logic. However, when dealing with low-quality MEMS-IMUs, it is common to neglect small error corrections that may not yield significant performance improvements, such as those related to the Earth's rotation. Consequently, a simplified version of the INS mechanization can be expressed as follows [3], [4]:

$$\begin{cases} \mathbf{r}_k^n = \mathbf{r}_{k-1}^n + \mathbf{v}_k^n \Delta t_k \\ \mathbf{v}_k^n = \mathbf{v}_{k-1}^n + \mathbf{C}_{b,k}^n \left(\Delta \mathbf{v}_k^b + \frac{\Delta \boldsymbol{\theta}_k^b \times \Delta \mathbf{v}_k^b}{2} \right) - \mathbf{g}^n \Delta t_k \\ \mathbf{C}_{b,k}^n = \mathbf{C}_{b,k-1}^n \left[\mathbf{I} + \Delta \boldsymbol{\theta}_k^b + \frac{\Delta \boldsymbol{\theta}_{k-1}^b \times \Delta \boldsymbol{\theta}_k^b}{12} \right] \end{cases} \quad (6)$$

where \mathbf{r}^n and \mathbf{v}^n are the position and velocity vectors in the n -frame, respectively; \mathbf{C}_b^n is the transformation matrix from the b -frame to the n -frame; $\mathbf{g}^n = [0, 0, -9.8]^T$ is Earth's gravity vector; $\Delta \mathbf{v}_k^b = (\tilde{\mathbf{f}}_k^b - \mathbf{b}_{f,k}) \Delta t_k$ is the velocity increment in the b -frame; $\tilde{\mathbf{f}}^b$ and \mathbf{b}_f are the acceleration and bias of the accelerometer, respectively; $\Delta \boldsymbol{\theta}_k^b = (\tilde{\boldsymbol{\omega}}_k^b - \mathbf{b}_{\omega,k}) \Delta t_k$ is the angle increment in the b -frame; $\tilde{\boldsymbol{\omega}}^b$ and \mathbf{b}_g are the angle rate and bias of the gyroscope, respectively; $\Delta t_k = t_k - t_{k-1}$ is the time interval between the $(k-1)$ -th and k -th epochs; and " \times " is the cross-product form of a vector.

B. Extended Kalman Filter

A error state Extended Kalman Filter (EKF) is used to fuse the inertial navigation and motion constraint information. The error state indicates the difference between the estimated and real values. The 18-dimensional error state variables at k moment are defined as

$$\mathbf{X} = [\delta \mathbf{r}^n \quad \delta \mathbf{v}^n \quad \boldsymbol{\phi} \quad \delta \mathbf{b}_\omega \quad \delta \mathbf{b}_f \quad \delta \mathbf{l}^b]^T \quad (7)$$

where $\delta \mathbf{r}^n$ and $\delta \mathbf{v}^n$ are the position and velocity error vectors in the n -frame, respectively; $\boldsymbol{\phi}$ is the attitude error vector; $\delta \mathbf{b}_\omega$ and $\delta \mathbf{b}_f$ are the bias error vectors of the gyroscope and accelerometer, respectively; $\delta \mathbf{l}^b$ is the lever arm error vector in the b -frame. The lever arm error is used as a parameter to be estimated in the filter because the user's height varies greatly, and an accurate lever arm cannot be obtained through manual measurement.

The gyroscope and accelerometer biases can be regarded as a first-order Markov process, the lever arm can be treated as a constant. Hence, the continuous system state model is derived as follows [8]

$$\dot{\mathbf{X}} = \mathbf{F}\mathbf{X} + \mathbf{G}\mathbf{W} \quad (8)$$

$$\mathbf{F} = \begin{bmatrix} \mathbf{0}_3 & \mathbf{I}_3 & \mathbf{0}_3 & \mathbf{0}_3 & \mathbf{0}_3 & \mathbf{0}_3 \\ \mathbf{0}_3 & \mathbf{0}_3 & \mathbf{f}^n \times & \mathbf{C}_b^n & \mathbf{0}_3 & \mathbf{0}_3 \\ \mathbf{0}_3 & \mathbf{0}_3 & \mathbf{0}_3 & \mathbf{0}_3 & -\mathbf{C}_b^n & \mathbf{0}_3 \\ \mathbf{0}_3 & \mathbf{0}_3 & \mathbf{0}_3 & -1/\tau_{b_f} & \mathbf{0}_3 & \mathbf{0}_3 \\ \mathbf{0}_3 & \mathbf{0}_3 & \mathbf{0}_3 & \mathbf{0}_3 & -1/\tau_{b_\omega} & \mathbf{0}_3 \\ \mathbf{0}_3 & \mathbf{0}_3 & \mathbf{0}_3 & \mathbf{0}_3 & \mathbf{0}_3 & \mathbf{0}_3 \end{bmatrix} \quad (9)$$

$$\mathbf{G} = \begin{bmatrix} \mathbf{0}_3 & \mathbf{0}_3 & \mathbf{0}_3 & \mathbf{0}_3 & \mathbf{0}_3 \\ \mathbf{C}_b^n & \mathbf{0}_3 & \mathbf{0}_3 & \mathbf{0}_3 & \mathbf{0}_3 \\ \mathbf{0}_3 & -\mathbf{C}_b^n & \mathbf{0}_3 & \mathbf{0}_3 & \mathbf{0}_3 \\ \mathbf{0}_3 & \mathbf{0}_3 & \mathbf{I}_3 & \mathbf{0}_3 & \mathbf{0}_3 \\ \mathbf{0}_3 & \mathbf{0}_3 & \mathbf{0}_3 & \mathbf{I}_3 & \mathbf{0}_3 \\ \mathbf{0}_3 & \mathbf{0}_3 & \mathbf{0}_3 & \mathbf{0}_3 & \mathbf{I}_3 \end{bmatrix}, \quad \mathbf{W} = \begin{bmatrix} \mathbf{w}_f \\ \mathbf{w}_\omega \\ \mathbf{w}_{b_f} \\ \mathbf{w}_{b_\omega} \\ \mathbf{w}_{l^b} \end{bmatrix} \quad (10)$$

where \mathbf{F} is the dynamic transform matrix; $\mathbf{f}^n \times$ is the skew-symmetric matrix of \mathbf{f}^n ; τ_{b_f} and τ_{b_ω} are the correlation times, which are set to 1800s; \mathbf{G} is the noise distribution matrix; and \mathbf{W} is the system noise, which is assumed to be zero-mean Gaussian white noise with the correlation covariance matrix \mathbf{Q} ; \mathbf{w}_f and \mathbf{w}_ω are the measurement white noises of the accelerometer and gyroscopes, respectively; \mathbf{w}_{b_f} and \mathbf{w}_{b_ω} are the driving white noises of the bias model; \mathbf{w}_{l^b} is the white noises of the lever arm model.

Because the MEMS IMU sampling interval Δt (0.005s) is very small, and $\mathbf{F}_k \Delta t \ll \mathbf{I}$, the discrete-time system state model can be derived as follows [23]

$$\mathbf{X}_k = \Phi_{k,k-1} \mathbf{X}_{k-1} + \mathbf{w}_{k-1} \quad (11)$$

$$\begin{cases} \Phi_{k,k-1} = \exp[\mathbf{F}_{k-1} \Delta t] \approx \mathbf{I}_{18} + \mathbf{F}_k \Delta t \\ \mathbf{Q}_k \approx \frac{\Delta t}{2} (\Phi_{k,k-1} \mathbf{G}_{k-1} \mathbf{Q} \mathbf{G}_{k-1}^T \Phi_{k,k-1}^T + \mathbf{G}_k \mathbf{Q} \mathbf{G}_k^T) \end{cases} \quad (12)$$

where $\Phi_{k,k-1}$ is the discrete transform matrix, \mathbf{Q}_k is the covariance matrix of the discrete system noise \mathbf{w}_{k-1} , \mathbf{I}_{18} is an 18-dimensional identity matrix.

C. Zero Observation Model

1) *Lever Arm based Zero Position Increment Update (LA-ZPIU)*: When Eq. 4 and Eq. 5 are both true, the velocity of the ankle should be zero. Based on this assumption, we construct a zero-velocity observation vector

$$\hat{\mathbf{v}}_{ankle}^n = [0 \ 0 \ 0]^T + \mathbf{n}_{v^n} \quad (13)$$

where \mathbf{n}_{v^n} is measurement noise. By performing the perturbation analysis, Eq. 1 can be written as

$$\begin{aligned} \hat{\mathbf{v}}_{ankle}^n &= \hat{\mathbf{v}}^n + \hat{\mathbf{C}}_b^n (\hat{\boldsymbol{\omega}}^b \times) \hat{\mathbf{l}}^b \\ &\approx \mathbf{v}^n + \delta \mathbf{v}^n \\ &\quad + (\mathbf{I} - \boldsymbol{\phi} \times) \mathbf{C}_b^n (\boldsymbol{\omega}^b \times - \delta \mathbf{b}_\omega \times) (\mathbf{l}^b + \delta \mathbf{l}^b) \\ &\approx \mathbf{v}^n + \delta \mathbf{v}^n + (\mathbf{C}_b^n \boldsymbol{\omega}^b \times \mathbf{l}^b) \times \boldsymbol{\phi} \\ &\quad - \mathbf{C}_b^n (\mathbf{l}^b \times) \delta \mathbf{b}_\omega + \mathbf{C}_b^n (\boldsymbol{\omega}^b \times) \delta \mathbf{l}^b \end{aligned} \quad (14)$$

Then, the velocity error observation equation in the n -frame can be written as

$$\begin{aligned} \delta \mathbf{z}_{v^n} &= \hat{\mathbf{v}}_{ankle}^n - \tilde{\mathbf{v}}_{ankle}^n \\ &= \hat{\mathbf{v}}_{ankle}^n - ([0 \ 0 \ 0]^T + \mathbf{n}_{v_{ankle}^n}) \\ &\approx \delta \mathbf{v}^n + (\mathbf{C}_b^n \boldsymbol{\omega}^b \times \mathbf{l}^b) \times \boldsymbol{\phi} - \mathbf{C}_b^n (\mathbf{l}^b \times) \delta \mathbf{b}_\omega \\ &\quad + \mathbf{C}_b^n (\boldsymbol{\omega}^b \times) \delta \mathbf{l}^b - \mathbf{n}_{v^n} \end{aligned} \quad (15)$$

To address the issue of increased velocity noise and the subsequent degradation of positioning performance caused by the larger fluctuations of the shin compared to the foot, we introduce a position observation model based on the constraint that the ankle position remains unchanged during the static period. This constraint implies that the position increment of the ankle during the static period should be zero. We can express the position increment observation equation in the n -frame as follows

$$\delta \mathbf{z}_{\Delta r^n} = \Delta \hat{\mathbf{r}}_{ankle}^n - \Delta \tilde{\mathbf{r}}_{ankle}^n \quad (16)$$

where $\Delta \hat{\mathbf{r}}_{ankle}^n$ and $\Delta \tilde{\mathbf{r}}_{ankle}^n$ is the predicted and observed position increments in the n -frame. Substitute Eq. 15 into Eq. 16 to get

$$\begin{aligned} \delta \mathbf{z}_{\Delta r^n} &= \int_{t_{k-1}}^{t_k} \hat{\mathbf{v}}_{ankle}^n dt - \int_{t_{k-1}}^{t_k} \tilde{\mathbf{v}}_{ankle}^n dt \\ &\approx \int_{t_{k-1}}^{t_k} \delta \mathbf{v}^n dt + \int_{t_{k-1}}^{t_k} (\mathbf{C}_b^n \boldsymbol{\omega}^b \times \mathbf{l}^b) \times \boldsymbol{\phi} dt \\ &\quad - \int_{t_{k-1}}^{t_k} \mathbf{C}_b^n (\mathbf{l}^b \times) \delta \mathbf{b}_\omega dt + \int_{t_{k-1}}^{t_k} \mathbf{C}_b^n (\boldsymbol{\omega}^b \times) \delta \mathbf{l}^b dt \\ &\quad - \int_{t_{k-1}}^{t_k} \mathbf{n}_{v^n} dt \end{aligned} \quad (17)$$

Assuming that the influence of system noise is small in a short period of time (e.g., 0.3 seconds, the error of the state variable can be considered to be a constant [38]. Solving Eq. 16 using the rectangular integration method gives

$$\begin{aligned} \delta \mathbf{z}_{\Delta r^n} &\approx \sum_{i=1}^N \mathbf{I}_3 \Delta t_i \delta \mathbf{v}^n + \sum_{i=1}^N (\mathbf{C}_{b,i}^n \boldsymbol{\omega}_i^b \times \mathbf{l}_i^b) \times \Delta t_i \boldsymbol{\phi} \\ &\quad - \sum_{i=1}^N \mathbf{C}_{b,i}^n (\mathbf{l}_i^b \times) \Delta t_i \delta \mathbf{b}_\omega + \sum_{i=1}^N \mathbf{C}_{b,i}^n (\boldsymbol{\omega}_i^b \times) \Delta t_i \delta \mathbf{l}^b \\ &\quad - \mathbf{n}_{\Delta r^n} \end{aligned} \quad (18)$$

where N is the number of epochs in the static period $[t_{k-1}, t_k]$, $\mathbf{n}_{\Delta r^n}$ is observation noise.

2) *Zero Velocity Update (ZUPT)*: When the user is standing, the shin is also close to a static state. At this time, the observability of the lever arm will be severely reduced, and LA-ZPIU will cause the estimated lever arm to deviate from the real value. To avoid this problem, the zero-velocity update will be triggered when Eq. 4 and Eq. 5 are satisfied for more than 1 second. The velocity observation equation in the n -frame [3] is given by

$$\begin{aligned} \delta \mathbf{z}_{v^n} &= \hat{\mathbf{v}}^n - \tilde{\mathbf{v}}^n \\ &= \hat{\mathbf{v}}^n - ([0 \ 0 \ 0]^T + \mathbf{n}_{v^n}) \\ &\approx \delta \mathbf{v}^n - \mathbf{n}_{v^n} \end{aligned} \quad (19)$$

where \mathbf{n}_{v^n} is observable noise. At the same time, assuming that the change of the heading is caused by the integral of the gyroscope (i.e., ZIHR), the corresponding heading observation equation in the n -frame [3] is given by

$$\begin{aligned} \delta \mathbf{z}_\psi &= \hat{\psi} - \tilde{\psi}_{store} \\ &= \psi + \delta \psi - (\psi + n_\psi) \\ &= \begin{bmatrix} \frac{\partial \psi}{\partial \phi_x} & \frac{\partial \psi}{\partial \phi_y} & \frac{\partial \psi}{\partial \phi_z} \end{bmatrix} \boldsymbol{\phi} - n_\psi \\ &= \begin{bmatrix} \mathbf{C}_{11} \mathbf{C}_{31} & \mathbf{C}_{21} \mathbf{C}_{31} & -1 \end{bmatrix} \boldsymbol{\phi} - n_\psi \end{aligned} \quad (20)$$

where ψ_{store} is the heading corresponding to the first epoch of the stationary period, \mathbf{C}_{ij} is the element at row i and column j of \mathbf{C}_b^n , n_ψ is observable noise.

V. EXPERIMENTAL RESULTS

A. Test Description

Figure 4 illustrates the positional relationship of the sensors worn by the tester, including the foot, shin, and back. The inertial modules are positioned at the heel and the shin, respectively. Additionally, a GNSS receiver is installed in the backpack. The inertial module utilized in the experiment was developed by the WHU-i2Nav team and comprises a MEMS IMU, power module, Bluetooth low energy module, memory module (SD card), and a powerful general-purpose multi-protocol system-on-chip. To achieve time synchronization between multiple devices, time stamps are transmitted to smartphones via Bluetooth. Table I provides an overview of the main technical characteristics of the inertial module. As the test area is an open sky environment, GNSS offers a position reference with centimeter-level accuracy for evaluating the performance of the positioning system.



Fig. 4: The relative positional relationship between foot-mounted IMU, shin-mounted IMU, and GNSS receiver.

TABLE I: Main characteristics of the inertial module

Parameters	Gyroscope	Accelerometer
Data rate	200 Hz	200 Hz
Dynamic range	2000 °/s	16 g
Bias instability	10 °/h	0.2 mg
White noise	0.24 °/√h	0.06 m/s/√h
Weight		≈ 50 g
Size (no shell)		32 × 25 × 12 mm
Battery power	continuous work for more than 10 hours	

We conducted a positioning performance evaluation of four different schemes, namely:

1) Foot-INS: This scheme utilizes zero-velocity update (ZUPT) and zero-integrated heading rate (ZIHR), without incorporating additional observations such as linear constraints or magnetometer observations based on user-specific motion trajectory shapes and positioning environments [8].

2) Step-Shin-INS: This scheme is based on the empirical step model for pedestrian dead reckoning (PDR) [3].

3) ZUPT-Shin-INS: This scheme incorporates lever arm compensation-based zero velocity update (ZUPT) as described in Equation 14.

4) ZPIU-Shin-INS: This scheme employs lever arm compensation-based zero position increment update (ZPIU) as shown in Equation 15.

Since all four schemes are relative positioning methods, we aligned the initial 10-meter length of each test trajectory with the reference trajectory. This alignment process allows for the initialization of position and heading for the different schemes.

We conducted a comprehensive evaluation of the proposed method's positioning performance using both simple and complex walking states. The simple walking state involved users walking in the direction they were facing, including straight-line trajectories and polygonal trajectories. On the other hand, the complex walking state included users walking forward, walking sideways, and walking laterally, introducing more challenging scenarios for position estimation. By evaluating the proposed method under different walking states, we aimed to assess its robustness and accuracy in various real-world pedestrian navigation scenarios.

B. Simple Walking Test

1) *Straight-line Trajectory*: We conducted 16 tests on a 50-meter-long straight runway, with 4 testers (3 males and 1 female) walking the same straight trajectory 4 times. The trajectories estimated by using Foot-INS, Step-Shin-INS, ZUPT-Shin-INS, and ZPIU-Shin-INS are shown in Figure 5. To evaluate the accuracy of the position estimation, we calculated the end position errors for each scheme. Figure 6 presents the end position errors of the 16 test trajectories for the four schemes. The average end position errors across the 16 tests are as follows: 1.26m for Foot-INS, 7.30m for Step-Shin-INS, 1.21m for ZUPT-Shin-INS, and 1.05m for ZPIU-Shin-INS. These results indicate that the proposed ZPIU-Shin-INS scheme outperforms the other schemes in terms of accuracy, with the lowest average end position error among the four tested methods.

Among the four schemes evaluated, Step-Shin-INS shows the worst positioning performance. This can be attributed to the limitations of the empirical step model, which fails to accurately estimate the user's walking distance due to variations in factors such as height and weight. On the other hand, Foot-INS, ZUPT-Shin-INS, and ZPIU-Shin-INS achieve accurate estimation of the user's walking distance by employing periodic zero-velocity correction. This is mainly possible due to the high short-term relative positioning accuracy provided by the strapdown inertial navigation algorithm. Both ZUPT-Shin-INS and ZPIU-Shin-INS demonstrate similar positioning performance to Foot-INS, indicating that a shin-mounted IMU can replace a foot-mounted IMU without sacrificing accuracy. This offers improved convenience for pedestrian dead reckoning systems. Furthermore, ZPIU-Shin-INS outperforms ZUPT-Shin-INS in terms of positioning performance. This is because the shin is not strictly a rigid body affected by muscles, making it difficult to satisfy the assumption of zero-velocity correction. The position increment method used in ZPIU-Shin-INS mitigates the impact of instantaneous violations of the zero-velocity assumption by integrating velocity over a period of time. This improves the observability of the lever-

arm parameters and enables more precise estimation of the walking distance.

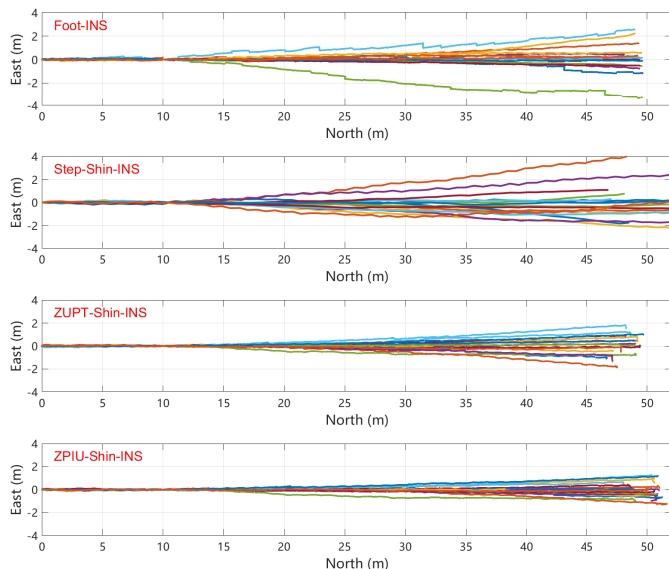


Fig. 5: The estimated 50-m straight-line trajectories in 16 tests.

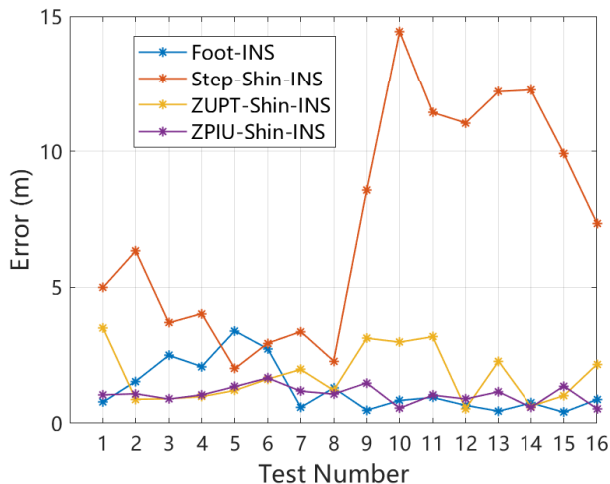


Fig. 6: End point position error of the estimated 50-m straight-line trajectories in 16 tests.

2) *Polygon Trajectory*: We conducted 4 polygon trajectory tests, with each test performed by a different user. The estimated trajectories using Foot-INS, Step-Shin-INS, ZUPT-Shin-INS, and ZPIU-Shin-INS are shown in Figure 7. To evaluate the position error of these trajectories, we plot the cumulative density function (CDF) of the position error in Figure 8. Step-Shin-INS exhibits more significant distance estimation errors and heading drift errors when following polygonal trajectories compared to straight-line trajectories. This can be attributed to the challenges posed by turning trajectories, which introduce inaccuracies in the step length model. Additionally, the shin-mounted IMU is subject to unpredictable external accelerations during complex trajectories, further degrading the performance. The accelerometer observations alone are insufficient to accurately estimate the

horizontal attitude, leading to increased heading drift rate. In contrast, Foot-INS, ZUPT-Shin-INS, and ZPIU-Shin-INS demonstrate similar positioning errors, regardless of whether the trajectory is straight or polygonal. This suggests that the zero-velocity correction methods are robust to the shape of the test trajectory. They effectively compensate for position estimation errors and maintain accuracy, regardless of the path followed by the user.

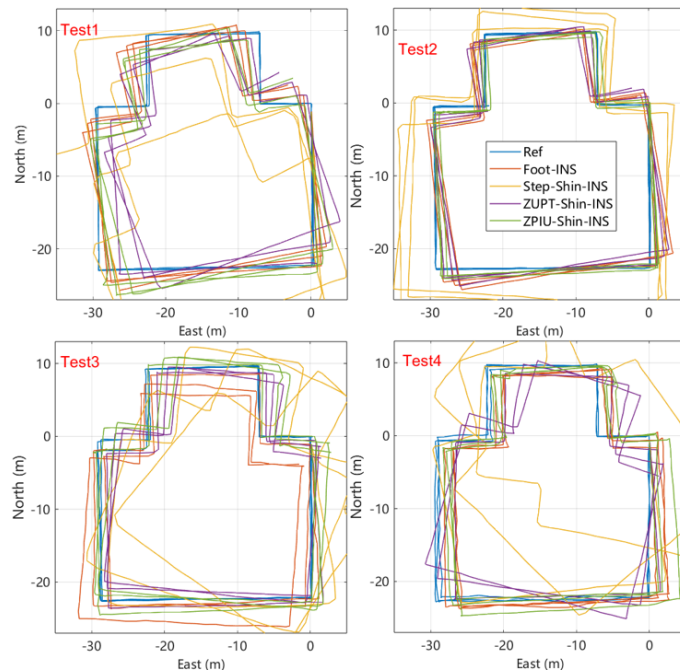


Fig. 7: The estimated polygon trajectories in 4 tests.

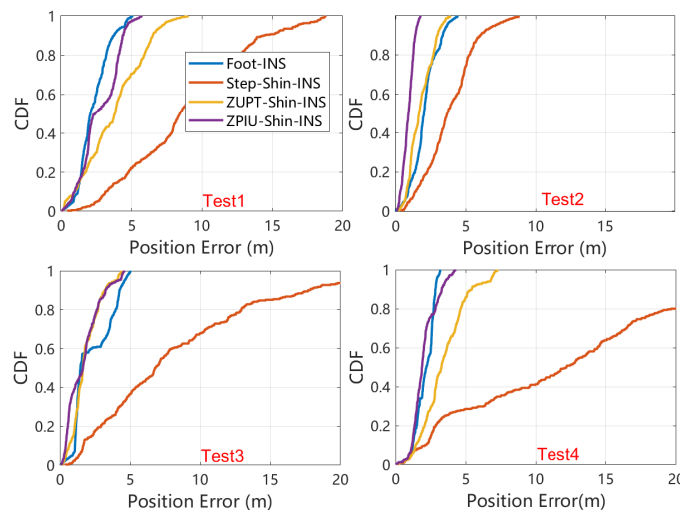


Fig. 8: Cumulative density function (CDF) of the position error of the estimated polygon trajectories in 4 tests.

Table II provides statistics on the position error of the polygon trajectory estimated by Foot-INS, Step-Shin-INS, ZUPT-Shin-INS, and ZPIU-Shin-INS in the 4 tests. The averaged position errors of Foot-INS are 2.20m (Mean), 2.75m (68%), and 3.87m (95% confidence level). For Step-Shin-INS, the averaged position errors are 7.79m, 9.45m, and

17.19m, respectively. ZUPT-Shin-INS yields averaged position errors of 2.78m, 3.43m, and 5.15m, while ZPIU-Shin-INS achieves averaged position errors of 1.71m, 2.11m, and 3.24m. Compare with ZUPT-Shin-INS, the mean positioning error of ZPIU-Shin-INS is reduced by 38%, indicating a greater improvement in positioning performance compared to a straight-line trajectory. This improvement can be attributed to the fact that complex user movements, such as turning, lead to more pronounced shaking, which affects the accuracy of ZUPT-based methods. Additionally, the average position error of ZPIU-Shin-INS is 0.5m smaller than that of Foot-INS. This can be attributed to the foot-mounted IMU experiencing significant sensor dynamic errors due to hard contact with the ground and large motion state changes. Lever-arm compensation enables accurate detection of the foot-ground contact period using ankle acceleration, which supports robust pedestrian positioning. In summary, ZPIU-Shin-INS demonstrates a higher level of positioning performance improvement compared to both straight-line trajectories and Foot-INS. The accuracy achieved by leveraging ankle acceleration for foot contact detection is sufficient for robust pedestrian positioning.

TABLE II: Position error statistics of the estimated polygon trajectories in 4 tests.

Test	Foot-INS			Step-Shin-INS			ZUPT-Shin-INS			ZPIU-Shin-INS		
	Mean	68%	95%	Mean	68%	95%	Mean	68%	95%	Mean	68%	95%
1	2.32	2.81	4.54	8.77	10.24	16.77	4.36	5.35	7.49	2.76	3.86	4.74
2	2.07	2.32	3.66	3.86	4.77	7.21	1.79	2.24	3.32	0.90	1.12	1.54
3	2.30	3.43	4.61	8.31	10.16	21.96	2.27	2.83	4.18	1.67	2.11	4.12
4	2.11	2.58	2.93	13.06	16.08	32.84	3.37	4.09	6.75	2.04	2.16	3.65
Mean	2.20	2.75	3.87	7.79	9.45	17.19	2.78	3.43	5.15	1.71	2.11	3.24

C. Complex Walking Test

In the complex walking test, the testers were instructed to switch their walking styles in the order of forward walking, sideways walking, and lateral walking. Since the heading of the sensor cannot be assumed to be consistent with the walking direction in a complex walking state, Step-Shin-INS cannot accurately reconstruct the user's true motion trajectory. Therefore, the positioning performance of Step-Shin-INS is not evaluated in this case. Figure 9 displays the 4 complex walking trajectories estimated by Foot-INS, ZUPT-Shin-INS, and ZPIU-Shin-INS. Figure 10 presents the cumulative density function (CDF) of the position error for the estimated complex walking trajectories in the 4 tests. In test 1, there is a jump phenomenon on the left side of the trajectory estimated by ZUPT-Shin-INS. This jump can be attributed to the low dynamics of the foot during abnormal walking states, which may lead to misjudgment of the static state period. However, ZPIU-Shin-INS incorporates a delay processing mechanism to identify and mitigate misjudgment of the static state, resulting in improved estimation accuracy. Furthermore, it is observed that complex walking patterns do not exhibit significant anomalies in the trajectories estimated by all the methods, including Foot-INS, ZUPT-Shin-INS, and ZPIU-Shin-INS. This indicates that

the proposed methods can handle complex walking states effectively and provide accurate trajectory estimation without significant deviations or anomalies.

Table III presents the position error statistics of the complex trajectories estimated by Foot-INS, ZUPT-Shin-INS, and ZPIU-Shin-INS in the 4 tests. The average position errors of Foot-INS are 0.63m (Mean), 0.82m (68%), and 1.10m (95%), while those of ZUPT-Shin-INS are 0.90m, 1.27m, and 1.88m. For ZPIU-Shin-INS, the average position errors are 0.60m, 0.73m, and 1.22m. It is evident that the zero-velocity correction-based methods exhibit lower overall position errors in the complex trajectory tests compared to the simple trajectory scenario. This can be attributed to the increased contact time and reduced dynamics of the foot when walking sideways or laterally. Moreover, the positioning errors of ZPIU-Shin-INS and Foot-INS are nearly identical, indicating that the abnormal gait introduces a longer time zero-velocity corrections and complex dynamic interference.

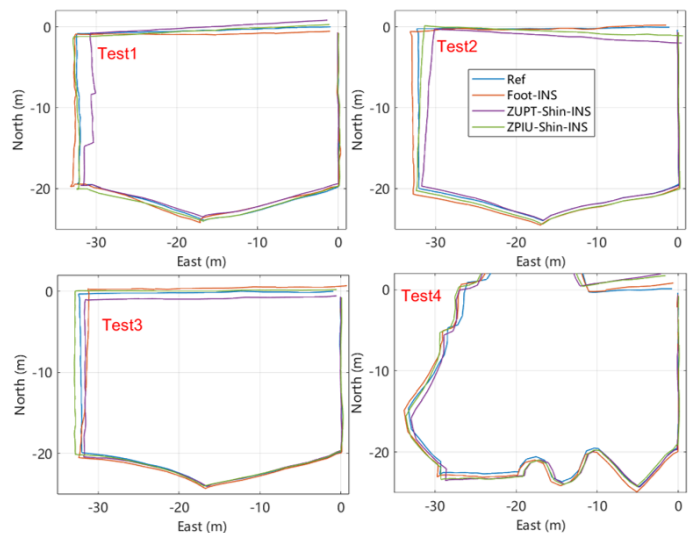


Fig. 9: The estimated complex walking trajectories in 4 tests.

TABLE III: Position error statistics of the estimated complex walking trajectories in 4 tests.

Test	Foot-INS			ZUPT-Shin-INS			ZPIU-Shin-INS		
	Mean	68%	95%	Mean	68%	95%	Mean	68%	95%
1	0.51	0.65	0.87	0.91	1.47	2.02	0.40	0.51	0.69
2	0.71	0.92	0.98	1.10	1.58	2.47	0.64	0.58	1.70
3	0.77	1.14	1.65	0.62	0.86	1.13	0.49	0.73	0.84
4	0.52	0.58	0.84	0.98	1.16	1.88	0.85	1.08	1.67
Mean	0.63	0.82	1.10	0.90	1.27	1.88	0.60	0.73	1.22

VI. DISCUSSION

The concept of Shin-INS involves projecting the velocity of a shin-mounted IMU onto the ankle, ensuring the physical feasibility of zero-velocity correction. The accuracy of the lever arm, which represents the positional relationship between the center of the shin-mounted IMU and the ankle, directly impacts the improvement in position performance achieved

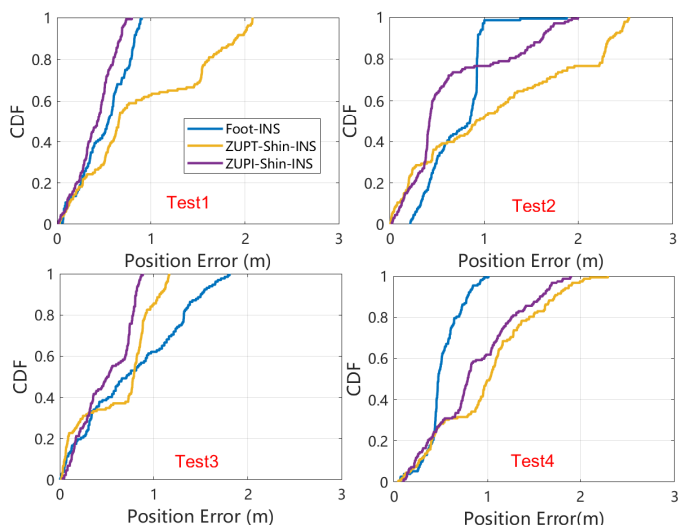


Fig. 10: Cumulative density function (CDF) of the position error of the estimated complex walking trajectories in 4 tests.

through zero-velocity correction. Therefore, real-time online estimation of the lever arm is essential in Shin-INS to account for variations in user height and IMU installation position.

Figure 11 illustrates the estimated lever arm and corresponding standard deviations obtained from a single test using the proposed method. The plot demonstrates that the lever arm exhibits good observability and remains stable after convergence. The standard deviation curve indicates that the lever arm is only observable during the user’s normal walking state, typically taking approximately 100 seconds (i.e., [50, 150] s) to converge. This can be attributed to the minimal rotation of the calf around the ankle during foot contact and the significant influence of sensor noise and calf muscle interference. Hence, ensuring a sufficient convergence time is crucial for achieving optimal performance in Shin-INS.

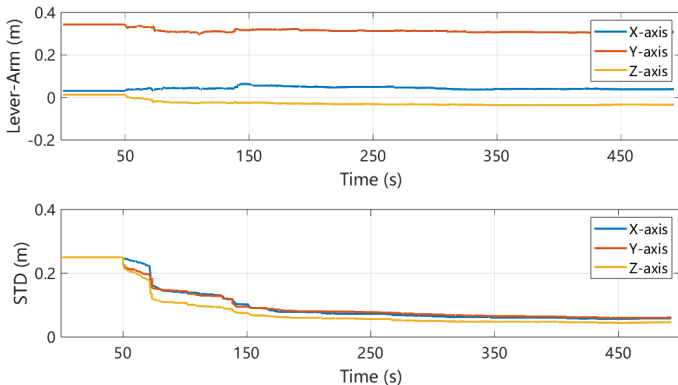


Fig. 11: The estimated 50-m straight-line trajectories in 16 tests.

In general, when the initial values of the lever arm parameters are reasonably accurate, Shin-INS can achieve comparable positioning performance and applicability to Foot-INS. One advantage of Shin-INS is that it does not rely on customized shoes, making it more user-friendly for ordinary individuals. However, in the initialization stage, if the lever arm parameters

are unknown, the positioning performance of Shin-INS can be significantly compromised. In this scenario, Shin-INS cannot match the positioning performance of Foot-INS while still maintaining its plug-and-play feature.

VII. CONCLUSIONS AND FUTURE WORK

This paper presents a novel shin-mounted inertial navigation system (Shin-INS) utilizing an IMU. Shin-INS employs lever arm compensation in conjunction with shin-IMU measurements to derive ankle acceleration. It introduces a static state detector that improves the accuracy of zero-velocity interval estimation compared to traditional methods. Additionally, a lever-arm compensation-based zero position incremental update method (LA-ZPIU) is proposed to enhance position estimation robustness by mitigating disturbances caused by calf muscles. The experimental results obtained from both normal and abnormal walking tests demonstrate that Shin-INS achieves positioning performance that is comparable to Foot-INS. In summary, Shin-INS effectively enhances the convenience of system installation without compromising performance.

This paper primarily focuses on analyzing the positioning performance of Shin-INS during normal walking speeds. However, there is still a need to investigate the performance of Shin-INS in complex pedestrian gaits and challenging positioning environments. In future research, it is recommended to conduct further evaluations of Shin-INS in scenarios involving running and on uneven terrain to assess its positioning capabilities under these conditions. Additionally, efforts should be made to enhance the robustness of the positioning system to ensure reliable performance in various real-world scenarios.

REFERENCES

- [1] N. El-Sheimy and Y. Li, “Indoor navigation: State of the art and future trends,” *Satellite Navigation*, vol. 2, no. 1, pp. 1–23, 2021.
- [2] N. El-Sheimy and A. Youssef, “Inertial sensors technologies for navigation applications: State of the art and future trends,” *Satellite Navigation*, vol. 1, no. 1, pp. 1–21, 2020.
- [3] J. Kuang, X. Niu, and X. Chen, “Robust pedestrian dead reckoning based on mems-imu for smartphones,” *Sensors*, vol. 18, no. 5, p. 1391, 2018.
- [4] X. Niu, T. Liu, J. Kuang, and Y. Li, “A novel position and orientation system for pedestrian indoor mobile mapping system,” *IEEE Sensors Journal*, vol. 21, no. 2, pp. 2104–2114, 2020.
- [5] S. Beauregard and H. Haas, “Pedestrian dead reckoning: A basis for personal positioning,” in *Proceedings of the 3rd Workshop on Positioning, Navigation and Communication*, 2006, pp. 27–35.
- [6] A. R. Jimenez, F. Seco, C. Prieto, and J. Guevara, “A comparison of pedestrian dead-reckoning algorithms using a low-cost mems imu,” in *2009 IEEE International Symposium on Intelligent Signal Processing*. IEEE, 2009, pp. 37–42.
- [7] E. Foxlin, “Pedestrian tracking with shoe-mounted inertial sensors,” *IEEE Computer graphics and applications*, vol. 25, no. 6, pp. 38–46, 2005.
- [8] X. Niu, T. Liu, J. Kuang, Q. Zhang, and C. Guo, “Pedestrian trajectory estimation based on foot-mounted inertial navigation system for multistory buildings in postprocessing mode,” *IEEE Internet of Things Journal*, vol. 9, no. 9, pp. 6879–6892, 2021.
- [9] J. Kuang, T. Li, Q. Chen, B. Zhou, and X. Niu, “Consumer-grade inertial measurement units enhanced indoor magnetic field matching positioning scheme,” *IEEE Transactions on Instrumentation and Measurement*, vol. 72, pp. 1–14, 2022.
- [10] L. E. Díez, A. Bahillo, J. Otegui, and T. Otim, “Suitability analysis of wrist-worn sensors for implementing pedestrian dead reckoning systems,” *IEEE Sensors Journal*, vol. 18, no. 12, pp. 5098–5114, 2018.

- [11] Y. Tian, A. Peng, X. Xu, and W. Zhang, "A heading estimation algorithm for wrist device assisted by sequential geomagnetic observations," *IEEE Sensors Journal*, vol. 22, no. 6, pp. 5309–5317, 2021.
- [12] S. Beauregard, "A helmet-mounted pedestrian dead reckoning system," in *3rd International Forum on Applied Wearable Computing 2006*. VDE, 2006, pp. 1–11.
- [13] C. Lu, H. Uchiyama, D. Thomas, A. Shimada, and R.-i. Taniguchi, "Indoor positioning system based on chest-mounted imu," *Sensors*, vol. 19, no. 2, p. 420, 2019.
- [14] N. Yu, Y. Li, X. Ma, Y. Wu, and R. Feng, "Comparison of pedestrian tracking methods based on foot-and waist-mounted inertial sensors and handheld smartphones," *IEEE Sensors Journal*, vol. 19, no. 18, pp. 8160–8173, 2019.
- [15] E. M. Diaz and A. L. M. Gonzalez, "Step detector and step length estimator for an inertial pocket navigation system," in *2014 International Conference on Indoor Positioning and Indoor Navigation (IPIN)*. IEEE, 2014, pp. 105–110.
- [16] Z.-A. Deng, G. Wang, Y. Hu, and D. Wu, "Heading estimation for indoor pedestrian navigation using a smartphone in the pocket," *Sensors*, vol. 15, no. 9, pp. 21518–21536, 2015.
- [17] S. Shin, C. Park, J. Kim, H. Hong, and J. Lee, "Adaptive step length estimation algorithm using low-cost mems inertial sensors," in *2007 IEEE sensors applications symposium*. IEEE, 2007, pp. 1–5.
- [18] H. Weinberg, "Using the adxl202 in pedometer and personal navigation applications," *Analog Devices AN-602 application note*, vol. 2, no. 2, pp. 1–6, 2002.
- [19] J. W. Kim, H. J. Jang, D.-H. Hwang, and C. Park, "A step, stride and heading determination for the pedestrian navigation system," *Journal of Global Positioning Systems*, vol. 3, no. 1-2, pp. 273–279, 2004.
- [20] Q. Wang, L. Ye, H. Luo, A. Men, F. Zhao, and Y. Huang, "Pedestrian stride-length estimation based on lstm and denoising autoencoders," *Sensors*, vol. 19, no. 4, p. 840, 2019.
- [21] C. Combettes and V. Renaudin, "Walking direction estimation based on statistical modeling of human gait features with handheld mimu," *IEEE/ASME Transactions on Mechatronics*, vol. 22, no. 6, pp. 2502–2511, 2017.
- [22] N. Ratchatanantakit, O. Nonnarit, P. Sonchan, M. Adjouadi, A. Barreto *et al.*, "A sensor fusion approach to marg module orientation estimation for a real-time hand tracking application," *Information Fusion*, vol. 90, pp. 298–315, 2023.
- [23] T. Liu, J. Kuang, W. Ge, P. Zhang, and X. Niu, "A simple positioning system for large-scale indoor patrol inspection using foot-mounted ins, qr code control points, and smartphone," *IEEE Sensors Journal*, vol. 21, no. 4, pp. 4938–4948, 2020.
- [24] I. Skog, P. Handel, J.-O. Nilsson, and J. Rantakokko, "Zero-velocity detection—an algorithm evaluation," *IEEE transactions on biomedical engineering*, vol. 57, no. 11, pp. 2657–2666, 2010.
- [25] J. Wahlström, I. Skog, F. Gustafsson, A. Markham, and N. Trigoni, "Zero-velocity detection—a bayesian approach to adaptive thresholding," *IEEE Sensors Letters*, vol. 3, no. 6, pp. 1–4, 2019.
- [26] M. Ren, K. Pan, Y. Liu, H. Guo, X. Zhang, and P. Wang, "A novel pedestrian navigation algorithm for a foot-mounted inertial-sensor-based system," *Sensors*, vol. 16, no. 1, p. 139, 2016.
- [27] R. Zhang, H. Yang, F. Höflinger, and L. M. Reindl, "Adaptive zero velocity update based on velocity classification for pedestrian tracking," *IEEE Sensors journal*, vol. 17, no. 7, pp. 2137–2145, 2017.
- [28] X. Tian, J. Chen, Y. Han, J. Shang, and N. Li, "A novel zero velocity interval detection algorithm for self-contained pedestrian navigation system with inertial sensors," *Sensors*, vol. 16, no. 10, p. 1578, 2016.
- [29] M. Ma, Q. Song, Y. Li, and Z. Zhou, "A zero velocity intervals detection algorithm based on sensor fusion for indoor pedestrian navigation," in *2017 IEEE 2nd Information Technology, Networking, Electronic and Automation Control Conference (ITNEC)*. IEEE, 2017, pp. 418–423.
- [30] J.-O. Nilsson, A. K. Gupta, and P. Händel, "Foot-mounted inertial navigation made easy," in *2014 International Conference on Indoor Positioning and Indoor Navigation (IPIN)*. IEEE, 2014, pp. 24–29.
- [31] C.-S. Jao, A. A. Abdallah, C. Chen, M.-W. Seo, S. S. Kia, Z. M. Kassas, and A. M. Shkel, "Pindoc: Pedestrian indoor navigation system integrating deterministic, opportunistic, and cooperative functionalities," *IEEE Sensors Journal*, vol. 22, no. 14, pp. 14424–14435, 2022.
- [32] K. Abdulrahim, C. Hide, T. Moore, and C. Hill, "Using constraints for shoe mounted indoor pedestrian navigation," *The Journal of Navigation*, vol. 65, no. 1, pp. 15–28, 2012.
- [33] J. Borenstein, L. Ojeda, and S. Kwanmuang, "Heuristic reduction of gyro drift in imu-based personnel tracking systems," in *Optics and Photonics in Global Homeland Security V and Biometric Technology for Human Identification VI*, vol. 7306. SPIE, 2009, pp. 244–254.
- [34] A. R. Jiménez, F. Seco, F. Zampella, J. C. Prieto, and J. Guevara, "Improved heuristic drift elimination (ihde) for pedestrian navigation in complex buildings," in *2011 International Conference on Indoor Positioning and Indoor Navigation*. IEEE, 2011, pp. 1–8.
- [35] K. Abdulrahim, C. Hide, T. Moore, and C. Hill, "Aiding low cost inertial navigation with building heading for pedestrian navigation," *The Journal of Navigation*, vol. 64, no. 2, pp. 219–233, 2011.
- [36] G. Bailey and R. Harle, "Assessment of foot kinematics during steady state running using a foot-mounted imu," *Procedia Engineering*, vol. 72, pp. 32–37, 2014.
- [37] I. Skog, J.-O. Nilsson, P. Händel, and A. Nehorai, "Inertial sensor arrays, maximum likelihood, and cramér-rao bound," *IEEE Transactions on Signal Processing*, vol. 64, no. 16, pp. 4218–4227, 2016.
- [38] L. Wang, X. Niu, T. Zhang, H. Tang, and Q. Chen, "Accuracy and robustness of odo/hnc measurement models for wheeled robot positioning," *Measurement*, vol. 201, p. 111720, 2022.



Jian Kuang received the B.Eng. degree and Ph.D. degree in Geodesy and Survey Engineering from Wuhan University, Wuhan, China, in 2013 and 2019, respectively. He is currently an Associate Research Fellow with the GNSS Research Center in Wuhan University, Wuhan, China. His research interests focus on inertial navigation, pedestrian navigation and indoor positioning.



Dazhou Xia received the B.Eng. degrees in navigation engineering from Wuhan University, Wuhan, China, in 2022, where he is currently pursuing the master's degree in geodesy and surveying engineering. His research interests focus on inertial navigation, sensor fusion algorithms, pedestrian navigation and indoor positioning.

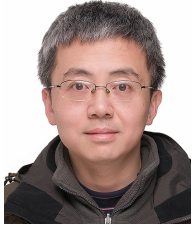


Tao Liu received the B.S. degree in Geographic Information System from Liaoning Technical University, Fuxin, China, in 2015, and M.S. degree in Surveying and Mapping from Liaoning Technical University, Fuxin, China, in 2018. He is currently pursuing the Ph.D. degree in GNSS Research Center, Wuhan University, Wuhan, China. His research interests focus on inertial navigation, sensor fusion algorithms, pedestrian navigation and indoor positioning.



Qijin Chen received the B.Eng. degree and Ph.D. degree in Geodesy and Survey Engineering from Wuhan University, Wuhan, China, in 2011 and 2016, respectively.

He is currently an Associate Research Fellow with the GNSS Research Center, Wuhan University, Wuhan, China. His research interests focus on INS with aiding and its applications in geodesy and precise surveying engineering including railway track geometry measuring and underground pipeline surveying.



Xiaoji Niu got his Ph.D. and bachelor degrees from the Department of Precision Instruments at Tsinghua University in 2002 and 1997 respectively.

He did post-doctoral research at the University of Calgary and worked as a senior scientist in SiRF Technology Inc. He is now a Professor of GNSS Research Center at Wuhan University in China. Dr. Niu leads a multi-sensor navigation group focuses on GNSS/INS integrations, low-cost navigation sensor fusion, and its new applications. Dr. Niu has published more than 90 academic papers and own 28 patents.